INTERNATIONAL JOURNAL FOR NUMERICAL AND ANALYTICAL METHODS IN GEOMECHANICS
Int. J. Numer. Anal. Meth. Geomech., **23**, 317–333 (1999)

A SEMI-ANALYTICAL MODEL FOR THE SIMULATION OF SOLUTE TRANSPORT IN A NETWORK OF FRACTURES HAVING RANDOM ORIENTATIONS

K. S. NOVAKOWSKI*, AND J. D. BOGAN†

National Water Research Institute, 867 Lakeshore Road, P.O. Box 5050, Burlington, Ontario, Canada L7R 4AB

SUMMARY

A semi-analytical model is developed which accounts for solute transport through a multi-dimensional network of fractures having random orientations and sparse distribution. Transport processes including hydrodynamic dispersion, matrix diffusion, retardation, decay and solute transfer at fracture intersections, are considered. The model is derived by application of the Laplace transform to the governing transport equation for each fracture element. The resulting ordinary differential equations are linked using robust descriptions of mass conservation at the fracture intersections. Solute concentrations are determined by numerically inverting the transformed equations in a sequential fashion. The model is verified using a formal mass balance and through comparison to existing solutions for solute transport in fractured media. To illustrate the use of the model, solute transport in a hypothetical network domain was simulated based on fracture conditions measured at a real field setting in a granitic rock. Copyright © 1999 John Wiley & Sons, Ltd.

Key words: analytical element; fracture network; solute transport; matrix diffusion; model

INTRODUCTION

Simulating the transport of contaminants in sparsely fractured media such as granites using models developed for porous media (i.e. a continuum approach) can be shown to be only applicable at a very large scale.[1] At the scale typical of a contaminant event, definition of the transport in each discrete fracture is required. In some cases, the groundwater flow system at this scale might be predominated by only one or two fracture features (such as one or two faults) and contaminant transport can be simulated using straightforward analytical models which account for solute transport in a single fracture (e.g. Reference 2). In cases where more than one or two fracture features influence the flow system, definition of the fractures is often conducted using stochastic or stochastic-deterministic methods in two dimensions and solute transport is solved in the resulting fracture network using particle-tracking methods.[3–5] For simple orthogonal networks, direct solution of the transport equations for both the fractures and the matrix can be undertaken using finite element methods.[6]

*Correspondence to: Dr. K. S. Novakowski, National Water Research Institute, 867 Lakeshore Rd., P.O. Box 5050, Burlington, Ontario, Canada L7R 4AB.
†Formerly with the Civil Engineering Department University of New Brunswick

Contract/grant Sponsor: Environment Canada

CCC 0363–9061/99/040317–17$17.50

Received 2 February 1998
Revised 13 April 1998

A computationally attractive alternative to these methods, for a multidimensional system of linked fracture elements, is the direct solution of the transport equations using analytical elements. In this case, variations of the solution of Tang *et al.*[2] in semi-analytical form are used in each fracture element and global concentrations are determined by simultaneous or sequential solution of the equation set. This method is less difficult to implement for non-orthogonal networks than finite-element methods (no discretization required in the matrix) and offers more flexibility than particle-tracking methods in accounting for transport processes such as matrix diffusion, multi-species transport and biological transformation.

Semi-analytical models for solute transport in a fracture network based on the solution of Tang *et al.*[2] have been developed by Rowe and Booker,[7,8] Mitchell and Sudicky[9] and Küpper *et al.*[10] Rowe and Booker[7,8] developed models to account for the transport of both conservative and reactive species limited to a two- or three-dimensional network of regularly spaced fractures. Transport followed only the regular fracture sets aligned in the direction of flow and mass transfer at fracture intersections was not considered. Küpper *et al.*[10] also developed a model for regular fracture arrangements, although mass transfer at fracture intersections was treated explicitly, in this case. To account for mass transfer, Küpper *et al.*[10] discretized the breakthrough curve in time for each element and used this as input to the next element down-gradient. Comparison of the model configured with several linked one-dimensional elements to the Tang *et al.* solution showed that errors accumulate according to the number of mass transfer events and the coarseness of the discretisation. In an unpublished study, Mitchell and Sudicky[9] used a Laplace transformed version of the Tang *et al.* solution (neglecting hydrodynamic dispersion) where mass transfer at fracture intersections was conducted using the equivalent of a Dirichlet boundary condition. Verification of the solution was not conducted.

Mixing at fracture intersections presents an additional problem associated with modeling two-dimensional fracture networks. There are a number of possible approaches including (1) assume complete mixing at each intersection, (2) transfer the solute mass according to stream tube routes at each intersection and (3) assume only partial diffusive exchange between stream tubes (i.e. Reference 11). Küpper *et al.*[10] determined that if it is assumed that only two fractures can intersect at a given point, out of the four possible flow combinations, three are mathematically equivalent for both stream tube routing and complete mixing conditions.

In this paper, a semi-analytical model is developed in which solute transport in a non-orthogonal fracture network is solved. Linear transport processes such as hydrodynamic dispersion, adsorption, decay and matrix diffusion are incorporated. The solution method involves derivation of transport equations for each fracture element by application of the Laplace transform. Virtually any transformable source function can be accommodated at any fracture location. Either complete mixing or stream tube routing and a rigorous definition of mass conservation is used at the fracture intersections. The equations are then solved sequentially using a propagation method. The model is verified by conducting a formal mass balance and by comparison to an existing analytical solution for matrix diffusion. To illustrate the use of the model, example simulations are undertaken in a sparsely fractured network typical of fractured crystalline rock.

MATHEMATICAL DEVELOPMENT

To derive a solution to solute transport in a fracture network, a fracture element, as depicted in Figure 1, is defined as the portion of a fracture that lies between the points of intersection with

other fractures or with a boundary. Thus, the spatial framework of the fracture system is represented by a set of saturated fracture elements connected at nodes within a homogenous and isotropic matrix. Groundwater flow is assumed to be steady and the aperture along each fracture is assumed to be constant, although variable aperture could easily be accommodated following the method of Nordqvist *et al.*[12] The groundwater velocity in each fracture element is determined using the method described by Rouleau[13] and Barker[14] for steady flow conditions.

In the following, a similar approach to that described by Barker[14] for transient groundwater flow in a network, is used to develop the solution for transport. The transport processes considered include advection, hydrodynamic dispersion, matrix diffusion, adsorption on the fracture surfaces and in the porous matrix, and first-order decay.

It is assumed that the porosity of the matrix is sufficiently small such that diffusing solute from adjacent fracture elements do not interact. This is clearly an approximation which will lead to an overestimate of the effect of matrix diffusion for some conditions. The approximation will be of most significance for simulations conducted in domains having short fracture elements and long periods of solute input.

Longitudinal dispersion is assumed to be constant and independent for each fracture element. Adsorption is assumed to be completely reversible and to follow a linear isotherm. Degradation follows a first-order decay process and occurs in both the matrix and the fracture at the same rate.

Solute concentration in a fracture element

The governing equations are formulated using constant coefficients for each discrete fracture element within a local co-ordinate system as shown in Figure 1. The equations are developed independently for the fracture and for the matrix and then coupled using a continuity condition between the fracture and the matrix following the method of Tang *et al.*[2] In Cartesian space, the governing equation for solute transport in a fracture element is (adapted from Tang *et al.*[2])

$$\frac{\partial c}{\partial t} + \frac{V}{R}\frac{\partial c}{\partial x} - \frac{\partial}{\partial x}\frac{D\partial c}{R\partial x} + \lambda c - \frac{\theta D'}{bR}\frac{\partial c'}{\partial z}\bigg|_{z=b} = 0 \tag{1}$$

where c and c' are the concentration of solute in the fracture element and the matrix, respectively, D' is the effective diffusion coefficient of the matrix (includes geometric properties of the pore space), D is the hydrodynamic dispersion coefficient, V is groundwater velocity, λ is the linear decay constant, θ is the porosity of the matrix, R is the retardation factor in the fracture, and b is 1/2 the fracture aperture ($2b/2$). The boundary and initial conditions are

$$c(x, 0) = 0 \tag{2}$$

$$c(\infty, t) = 0 \tag{3}$$

$$c(0, t) = c_i(t) \tag{4}$$

where $c_i(t)$ is the unknown inlet concentration. Note that a specified condition is not applied at the outlet boundary, located at $x = L$. Thus, it is assumed that the presence of the outlet boundary (i.e. a fracture intersection) has no influence on the solute concentration in the immediate vicinity up-gradient from the boundary. Based on the results of column experiments[15] conducted using outlet mixing conditions similar to that imparted by mixing at fracture intersections, this approximation is reasonable. Thus, the potential error incurred by this approximation

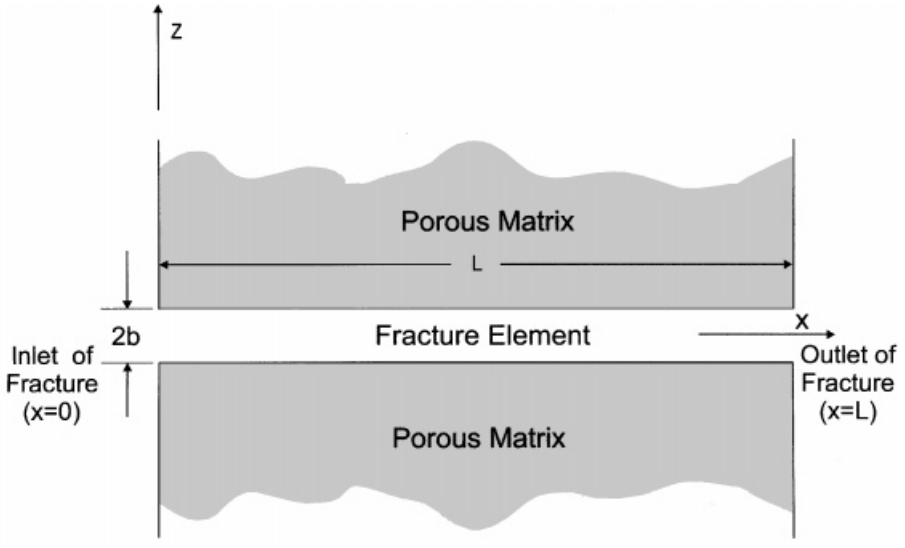

Figure 1. Schematic diagram of a fracture element and the surrounding porous matrix

is likely to be minimal in comparison to the approximation for matrix diffusion in the vicinity of fracture intersections, discussed above.

The differential equation for solute transport in the matrix is given as (after Tang *et al.*[2])

$$\frac{\partial c'}{\partial t} - \frac{D'}{R'}\frac{\partial^2 c'}{\partial z^2} + \lambda c' = 0 \tag{5}$$

where R' is the retardation factor in the matrix. The boundary and initial conditions for equation (5) are

$$c'(x,\ \infty, t) = 0 \tag{6}$$

$$c'(x, z, 0) = 0 \tag{7}$$

$$c'(x, b, t) = c(x, t) \tag{8}$$

To solve the system of equations (1)–(8), the Laplace transform method is employed. The solution for solute concentration in the fracture element is

$$\bar{c}(x, p) = \bar{c}_i(p) \exp\{vx(1 - E(p))\} \tag{9}$$

The Laplace transformed concentration in the fracture is given by $\bar{c}(x, p)$, $\bar{c}_i(p)$ is the Laplace transformed input condition, and

$$v = \frac{V}{2D} \tag{10}$$

and

$$E(p) = \sqrt{1 + \frac{4D}{V^2}\left(\frac{\theta\sqrt{D'R'(p+\lambda)}}{b} + R(p+\lambda)\right)} \tag{11}$$

The overbar indicates the Laplace transformed dependent variable, and p is the Laplace variable.

Flux between fracture elements

The transfer of mass between fracture elements is determined as a function of concentration at the fracture intersection. To preserve mass balance, it is necessary to include a dispersive flux term in addition to advective flux at the point of intersection. Thus, the equation that governs the mass flux of solute entering a fracture intersection is given by

$$J(L, t) = Vc(L, t) - D\frac{\partial c}{\partial x}(L, t) \tag{12}$$

where J is the mass flux term ($\mathrm{ML}^{-2}\,\mathrm{T}^{-1}$) that will be used in the assembly of equations for each fracture intersection. Substitution of equation (9) into the Laplace transform of (12) results in the final expression for the flux leaving a fracture element

$$\bar{J}(L, p) = \Phi(p)V\bar{c}_i(p)\,\mathrm{e}^{vL(1-E(p))} \tag{13}$$

where

$$\Phi(p) = \frac{1 + E(p)}{2} \tag{14}$$

Therefore, the flux exiting any fracture of length L is dependent only on the inlet concentration and the transport properties of that fracture element.

To determine the solute flux entering a given fracture from a fracture intersection, equation (12) is applied using a local co-ordinate of $x = 0$. Thus, the flux entering is given by

$$\bar{J}(0, p) = \Phi(p)V\bar{c}_i(p) \tag{15}$$

where $\Phi(p)$ is as given above.

Solute transport in a fracture network

Because the concentration of solute in a given fracture is dependent only on the inlet concentration for that fracture, a simple propagation method can be used to solve for the distribution of solute in the network. The nodes used to initiate the solution are usually those that constitute the most upgradient in the network. It is not necessary for there to be any solute input at these node, as the method propagates a null solution until solute input is encountered. However, because the application of solute input at non-mixing nodes cannot be directly implemented, solute input is limited to boundary nodes in order that general mixing conditions at interior fracture intersections can be utilized.

To formulate a complete solution, the mass flux entering and leaving each node must be summed. Both stream tube routing and complete mixing can be accounted for in this formulation. For example, Figure 2 shows the intersection of two fractures with two different flow arrangements. In Figure 2(a), contributing fractures and receiving fractures are opposite one another, while in Figure 2(b), contributing and receiving fractures are adjacent. The flow arrangements in Figures 2(a) and 2(b) can be classified as mixing and non-mixing (stream tube routing), respectively, according to the definitions given by Küpper *et al.*[10]

The nomenclature used in Figure 2 follows that developed by Barker.[14] The intersection node is given an integer value, i, and fracture elements connected to i are defined as j_1 through j_4. Any properties possessed by these fracture elements are given the subscript j. The fracture elements

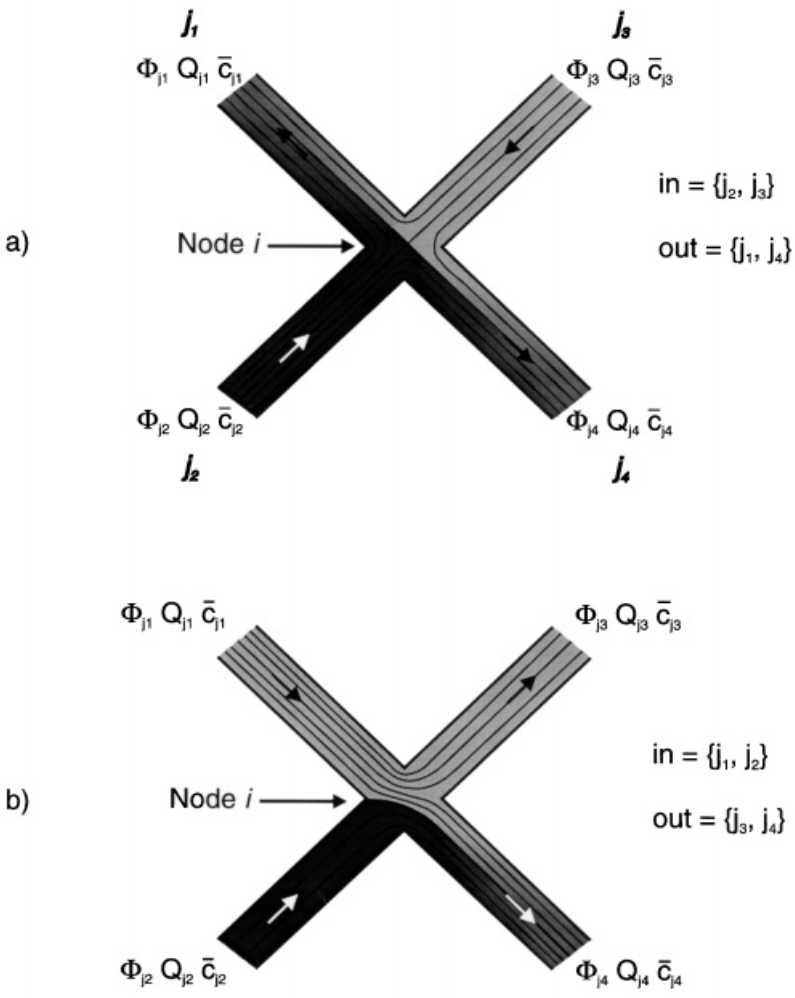

Figure 2. Examples of streamline routing at fracutre intersections. (a). Mixing case. Receiving fractures and contributing fractures are opposite one another (discontinuous intersection). (b). Non-mixing case. Receiving fractures and contributing fractures are adjacent to one another (continuous intersection). Nomenclature is arranged such that $Q_{j3} > Q_{j1}$.

defined as *in*, are those that supply flow, and the fracture elements defined as *out*, are those that receive flow.

Assuming no storage of solute at nodes, for uniform flux parallel to the fracture walls across a perpendicular cross-section, $2b_j w_j$, it can be shown that the mass balance at node i is

$$\sum_{j=\text{in}} J_{(\text{EX})j} 2b_j w_j = \sum_{j=\text{out}} J_{(\text{ENT})j} 2b_j w_j \tag{16}$$

where J_j is the flux to or from a fracture element, j, and w_j is the unit width of the fracture element. The (EX) subscript indicates that the solute is exiting from a fracture element, and the (ENT)

subscript indicates that solute is entering a receiving fracture element. Flux at the exit of an individual fracture element is determined from (13) as

$$\bar{J}_{(\mathrm{ENT})j} = \Phi_j(p) V_j \bar{c}_j(L_j, p) \tag{17}$$

where $\bar{c}_j(L_j, p)$ is the concentration leaving fracture element, j. Similarly, flux at the entrance to a fracture element is determined from equation (15) directly as

$$\bar{J}_{(\mathrm{ENT})j} = \Phi_j(p) V_j \bar{c}_i(p) \tag{18}$$

where $\bar{c}_i(p)$ is concentration at the node as calculated during the previous step (see below).

For the complete mixing case (i.e. Figure 2(a)), equations (17) and (18) are substituted into equation (16). This implies that all of the unknown concentrations contributed to receiving fracture elements from the node are equal at the inlets. Then $\bar{c}_i(p)$ is the concentration at the node after mixing has occurred (in the case of non-mixing conditions, this represents the mean concentration within the intersection). This allows us to rearrange the terms and to solve for $\bar{c}_i(p)$,

$$\bar{c}_i(p) = \frac{\sum_{j=\mathrm{in}} \Phi_j(p) Q_j \bar{c}_j(L_j, p)}{\sum_{j=\mathrm{out}} \Phi_j(p) Q_j} \tag{19}$$

where Q_j is the volumetric flow rate in the fracture element. Thus, for complete mixing, the outflow concentration from the node is given as

$$\bar{c}_j(0, p) = \bar{c}_i(p) j = \{\mathrm{out}\} \tag{20}$$

where $\bar{c}_j(0, p)$ and $\bar{c}_j(L, p)$ are concentrations located near the intersection, after solute concentration has become homogeneous within the fracture element.

The elements intersecting the inlet boundaries are treated differently as no inlet element is present. In this case, propagation of the solution is initiated with the first interior node and the concentration in the node on the boundary is set to zero (propagate a null solution) or to a Laplace transformable function. Viable inlet boundary conditions include Dirac, finite pulse, exponentially decaying and step-type functions.

For the one configuration (i.e. Figure 2(b)) that requires incomplete mixing (stream tube routing), a different formulation is applied, following the method suggested by Küpper *et al.*[10] For the example shown in Figure 2(b), $Q_{j1} > Q_{j3}$. In general, when determining concentrations at the intersection, the fracture numbering scheme is arranged so as to be consistent with this flow relation (i.e. the fractures are renumbered when $Q_{j1} < Q_{j3}$). For the case shown in Figure 2(b), the contribution of solute to fracture j_3 is exclusively from fracture j_1, therefore

$$\bar{c}_{j3}(0, p) = \bar{c}_{j1}(L_{j1}, p) \tag{21}$$

Equation (21) is substituted into (16) to determine the remaining inlet concentration. To avoid the problem of distributing external solute input at these types of intersections, as aforementioned, external solute input is limited to the boundary. Thus,

$$\bar{c}_{j4}(0, p) = \frac{[\Phi_{j1}(p) Q_{j1} - \Phi_{j3}(p) Q_{j3}] \bar{c}_{j1}(L, p) + \Phi_{j2}(p) Q_{j2} \bar{c}_{j2}(L, p)}{\Phi(p)_{j4} Q_{j4}} \tag{22}$$

To provide a comparison to models in which complete mixing is assumed at all fracture intersections, equation (22) can be replaced by equations (19) and (20).

To implement the solution, numerical inversion of the Laplace concentrations is required. This is conducted using the De Hoog *et al.*[16] algorithm. This algorithm has been evaluated for inversion of similar transport problems by Moench.[17] The results indicated that Peclet numbers (the ratio of distance over dispersivity) were limited to the range from 220 to 10,000 depending on the accuracy of the computer. Similar limitations were encountered in the present study, for the network solution. Further discussion of accuracy is provided in the following section.

Verification and mass balance

Verification of the model is based on comparison to the existing analytical solution of Tang *et al.*,[2] and on a formal mass balance conducted on components of transport in the fracture network. Further discussion of these verification procedures, including a comparison to the well-known Ogata–Banks solution, can be found in Reference 18.

To compare the network solutions given by equations (19) or (22), to the semi-analytical solution of Tang *et al.*,[2] a simple network configuration must be considered. For example, assume a segmented single fracture of length, L_t, bisected by one node located at the mid-point. Using a step function source of concentration at the inlet end and assuming that the aperture is the same in each segment, equation (19) can be reduced to

$$\bar{c}(L_t, p) = \frac{C_0}{p} \exp\{v(L_1 + L_2)(1 - E(p))\} \tag{23}$$

where L_1 and L_2 are the lengths of the fracture segments (i.e. $L_1 + L_2 = L_t$). Equation (23) is algebraically identical to equation (25) of Tang *et al.*[2] where L_t is equal to z.

Estimation of the total mass balance of solute in the fracture network is also helpful in verifying the mass-conservative nature of the model. To perform a formal mass balance at a given time, the following relationship must be evaluated

$$M_{\text{in}} = M_{\text{stored}} + M_{\text{out}} \tag{24}$$

where in the case of a network of fractures, M_{in} is the total mass of solute introduced into the network at system source nodes, M_{stored} is the total mass of solute stored in the fracture network and surrounding porous matrix, and M_{out} is the total mass of solute that has exited the network at exit boundary nodes. Exit boundary nodes are defined as those nodes that have no connected fracture elements to receive flow and thus are the points at which solute leaves the network.

For the purpose of performing the mass balance, only solute concentration in the fracture network is evaluated (i.e. matrix diffusion is not considered). Therefore, to determine the M_{stored} for the network, the mass stored in the each fracture element is determined by integration and then summed over the network. Because a spatially dependent equation for the concentration in each element has been developed, an integration performed on this equation with respect to volume yields the mass of solute. It is assumed that concentration is uniform through a lateral section, which allows the equation to be treated as a one-dimensional problem. Therefore, solute mass in a fracture element, $\bar{M}_j(p)$, can be defined in local co-ordinates as

$$\bar{M}_j(p) = 2b_j w_j \int_0^{L_j} \bar{c}_j(x, p)\mathrm{d}x \tag{25}$$

Substituting equation (9) into (25) and performing the integration yields

$$\bar{M}_j(p) = 2b_j w_j \frac{\bar{c}_j(0, p)}{v_j(1 - E_j(p))} (e^{vL_j(1 - E_j(p))} - 1) \tag{26}$$

To determine M_{in} and M_{out}, the cumulative mass of solute that has passed through entrance and exit nodes for the network, respectively, is determined. This mass is accumulated to a given time, $M_i(t)$, and may be evaluated by integrating the mass rate of flow over time as

$$M_i(t) = \int_0^t F_i(t)\, dt \tag{27}$$

If we perform a Laplace transform on this expression, we obtain

$$\bar{M}_i(p) = \frac{\bar{F}_i(p)}{p} \tag{28}$$

where $\bar{M}_i(p)$ is the Laplace transform of $M_i(t)$. M_{in} is determined by applying (27) directly at all system source nodes. M_{out} is estimated by applying (27) to all exit boundary nodes, where $\bar{F}_i(p)$ is determined by the addition of the mass rate of flow to the nodes in equation (15).

To evaluate the mass balance, numerical inversion of the Laplace concentration is required. Several example simulations were conducted using a stochastically generated fracture network to evaluate mass conservation. A mass balance was determined (following the procedure described above) to quantify the total error in the solution.

A series of stochastic networks of increasing fracture density were generated. Log variance of aperture was set to 0·1, in order to include a random component to the flow system. The domain was defined with a dimension in the direction of flow of twice that of the width. Boundary conditions were applied using a constant hydraulic head on the left- and right-hand sides of the network. A uniform gradient of 0·002 was induced across the network. The upper and lower boundaries were defined as no-flow. The dispersivity for each fracture ranged from 0·001 to 1·0 for individual realizations. Peclet numbers for the domain were calculated based on the mean path length across the domain. Relative error of the mass balance is expressed as

$$\text{Relative Error} = \left| \frac{(M_{out} + M_{stored}) - M^*_{in}}{M^*_{in}} \right| \tag{29}$$

where M^*_{in} is the simple addition of the mass of all Dirac inputs and is an exactly accurate figure. The error was determined for 10 snapshots in time for each network.

The maximum error for three realizations of the network having different fracture densities is shown in Figure 3. The total error exceeded the truncation error of the model ($1{\cdot}0 \times 10^{-6}$) at Peclet numbers of greater than 1000. This is consistent with the observations of Moench,[17] which suggests that the error observed at $Pe < 1000$ is introduced solely by the inversion scheme. The error increases in a logarithmic fashion at Pe greater than 1000. In addition, the concentration values at the exit nodes begin to show evidence of increasing 'noise' in the solution (random over- or underestimation of the concentration), usually at early times for these values of Pe. These limitations are generally encountered in the numerical implementation of inverse Laplace transforms at large Peclet numbers. However, it is important to note that error is small for the range of Pe below 1000. This range is more typical of real field conditions.

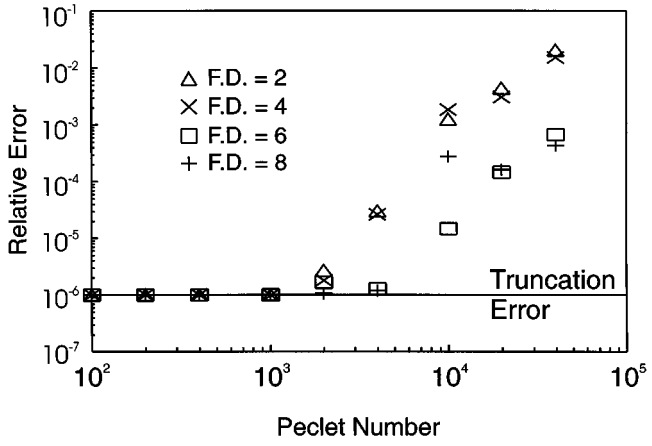

Figure 3. Relative error from simulations conducted in stochastically generated networks

Another, less easily measured source of error, is that related to approximation of the matrix diffusion process near fracture intersections. As aforementioned, this approximation should only generate significant errors where the fracture elements are short, and solute input is continuous and constant. For example, if an effective diffusion coefficient of $1{\cdot}2 \times 10^{-10}$ m^2/s for a salt tracer is assumed (e.g. Reference 19), the depth of penetration of the solute front (10 per cent of maximum concentration) into an unfractured medium will be only 0·3 m after five years of constant concentration in the fracture. Thus, for fractures in excess of 2–3 m length, the proportion of fracture length over which actual interference might occur will be less than 10 per cent and the model should incur minimal error.

RESULTS AND DISCUSSION

To illustrate the use of the model, example simulations are conducted whereby the structure of the fracture network closely follows that which might be found in crystalline rock. The purpose of these simulations is to demonstrate the efficiency of the model in testing conceptual models for fracture arrangement and for matrix diffusion.

Generation of fracture networks

Generation of the fracture network follows the stochastic method described by Rouleau.[13] First, length, orientation, and the location of the centre of the fractures are generated according to given fracture statistics. The lengths of the fractures are given a truncated exponential distribution.[20] To produce the exact linear density of fracture traces within the domain, the end-to-end fracture length is determined by multiplying the area of the domain by the fracture density, and the total generated fracture lengths are constrained to this value. In the following examples, two sets of fractures are stochastically generated, the orientations of which are determined from a separate mean and variance. Based on the mean and variance, a normal distribution function is

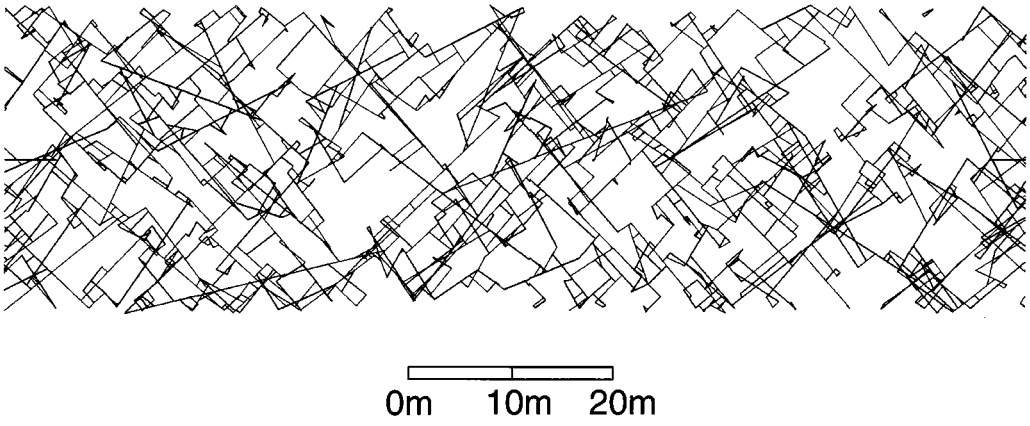

Figure 4. Example fracture network. Upper and lower boundaries are no-flow, while the left and right boundaries are constant head. Direction of flow is left to right

used to generate the orientation of the fracture. The apertures of each fracture set are given the properties of a log-normal distribution.

Intersections with boundaries and between fractures are then determined. The intersections that lie outside the specified domain are eliminated as are those that connect to dead-end fracture elements. The remaining intersections are defined as nodes in the flow path. Fracture elements are then determined, and the aperture of the parent fracture retained. In the final step, nodes are renumbered in order of position in the y direction. This reduces the bandwidth of the solution for flow by associating the spatial position with fracture connectivity, so that the difference in node numbers are more likely to be similar in integer value. An example of a stochastically generated network is shown in Figure 4.

The effect of sheeting fractures

Sheeting fractures often occur parallel to the ground surface in crystalline rock.[21] These fractures develop as extension features and are often of larger aperture and areal extent than the fractures in the surrounding area. In a field study conducted in monzonitic gneiss,[22] sheeting fractures were found to predominate the groundwater flow system at shallow depth. Interconnection between these features was controlled by fractures of smaller aperture and more random orientation. Thus, sheeting fractures form conduits for solute migration although macroscopic transport may be governing by the smaller fractures in the fracture framework. To investigate the effect that these fractures have on solute transport, several simple sheeting fracture arrangements are superimposed on a finer fracture network, and flow and transport are simulated. The placement of the sheeting fractures is conducted by locating the end co-ordinates in the desired positions on the existing stochastic framework.

A network with the properties given in Table I was combined with deterministically located fractures shown in the inset of Figures 5(a) and 5(b). The aperture of the deterministically placed fractures was set equal to 200 μm, and the porosity of the matrix was limited to zero. A Dirac source was introduced at the intersection of the leftmost sheeting fracture with the left-hand

Table I. Network and transport parameters used in the simulations

Network parameters and boundary conditions	
	Fracture density: 2·5 fractures / m
	Domain depth: 30 m
	Domain length: 100 m
	Mean aperture: 100 μm
	Log variance: 0·2
	Hydraulic gradient: 0·01
Transport parameters	
	Dispersivity: 0·5 m
	Matrix porosity: $\leqslant 1$ or 0%
	Matrix tortuosity: 0·1
	Diffusion coefficient: 6.1×10^{-5} m^2/d

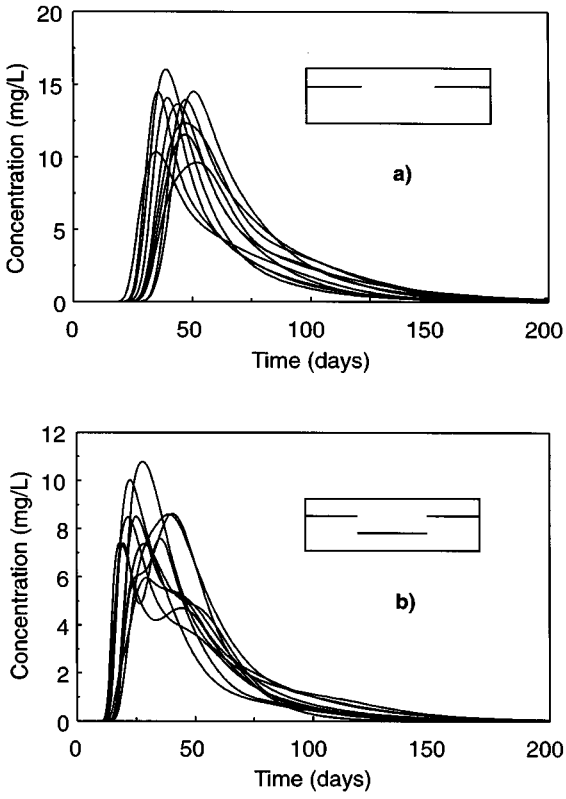

Figure 5. Breakthrough curves from simulations conducted in 10 network realizations. The inset diagram indicates the locations of the deterministically placed fractures in relation to the domain. Breakthrough curves are for (a) two sheeting fractures and (b) three sheeting fractures

boundary, and breakthrough was monitored at the exit of the rightmost sheeting fracture on the right-hand boundary. Flow was from left to right with reflection boundaries above and below. Errors as determined from mass balance calculations were negligible.

Figure 5(a) illustrates the results for 10 realizations. The shape of the breakthrough curves are uniformly asymmetrical, with significant tailing observed in some. The asymmetry arises due to transport in the fractures of smaller aperture. In addition, the time of peak arrival is dependent on the arrangement of the interconnections in the finer fracture sets. The breakthrough curve for the case in which the sheeting fracture is through-going and directly connects the entrance and exit (not shown) was observed to have a time to peak arrival of 4·0 days and a symmetrical shape. Thus, although rapid transport occurs in the sheeting fractures, the overall rate of migration is significantly limited by the fractures of smaller aperture.

Figure 5(b) illustrates a similar scenario in which a third sheeting fracture has been added (see inset). The presence of this fracture results in bi-modal distributions of concentration for some realizations. In addition, the time of arrival of the peak concentration, is much advanced relative to that shown in Figure 5(a). Thus, the arrangement of the sheeting fractures can have a profound effect on the transport properties of a domain such as this. To further investigate the occurrence of bi-modal distributions of concentration, Monte Carlo simulations with 50 realizations were conducted. The presence of bi-modal curves was observed at a frequency equivalent to that observed in Figure 5b. It is surmized that the presence of the third sheeting fracture led to multiple pathways for some realizations where one pathway followed the direct connection between each sheeting fracture and another followed the pathway through the fractures of smaller aperture joining the upper two sheeting fractures. Breakthrough curves having this shape have been observed in nature,[23] which suggests that fracture arrangements of this type may be common. It is important to note that a denser arrangement of sheeting fractures will smooth the breakthrough curves while a sparser arrangement of the vertical fractures will increase the irregular shape of the curves. Thus, the results of tracer experiments conducted over distances much greater than the average fracture length, in conjunction with the fracture statistics, should yield considerable information on the subsurface arrangement of fractures in crystalline rock environments.

Matrix diffusion

Because the present model is based on a semi-analytical solution, concentrations may be accurately determined over several orders of magnitude. This is useful when examining the influence of matrix diffusion. Tsang[24] investigated transport processes in fracture networks by simulating transport in a variety of configurations normally used for tracer experiments. Transport was simulated using particle tracking in a randomly generated network. At low concentrations, random noise was observed, making for a difficult interpretation of the transport processes at late times. However, on the basis of the results of several simulations, Tsang[24] proposed that concentrations in the tail of breakthrough curves for tracer experiments conducted in radial flow systems should follow a late-time dependence on $t^{-3/2}$.

In this study, several simulations were conducted to investigate these effects in a uniform flow field. The network domain and transport parameters are shown in Table I where matrix porosity ranged from 0 to 1 per cent. The value of the diffusion coefficient approximates that of an organic contaminant such as benzene. Deterministically placed sheeting fractures were not used in these simulations and the same realization of the fracture network was used for each run. The tracer (1·0 g) was introduced at the intersection of a fracture with the left-hand border. The progress of the solute was monitored across the entire exit boundary of the network (right-hand boundary) by multiplying the concentration in each fracture at the exit node by the volumetric flux leaving

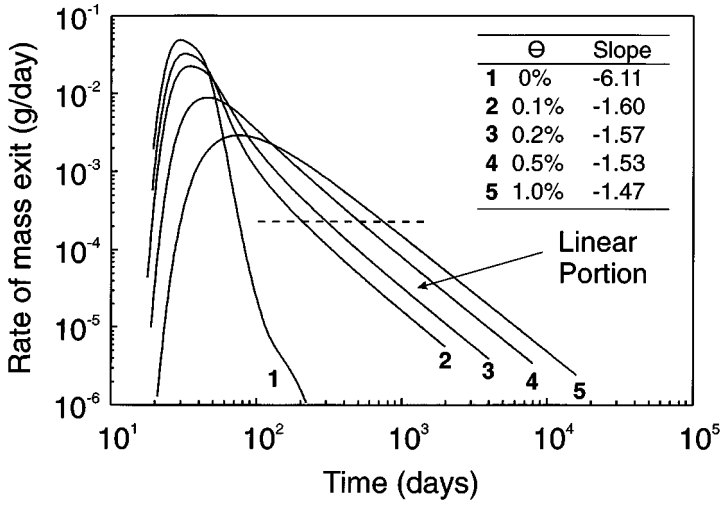

Figure 6. Log–log linearity in the tail of breakthough curves in a densely fractured network, due to matrix diffusion. Slopes approach a value of $-3/2$

that fracture and summing all contributions. Figure 6 illustrates the resultant mass rate of exit (g/day) for five simulations. The shape of these curves closely approximate the breakthrough curves for individual fractures.

Although mass flux through matrix diffusion across the exit boundary is not considered in this analysis, the error incurred by ignoring this component is likely negligible. This is because this process is only relevant to those fractures that might intersect the exit boundary at angles close to parallel with the boundary, of which there are very few for most network realizations. In addition, the rate of mass transfer across the exit boundary through the matrix from these fractures will only be a fraction of the percentage of mass flux exiting due to advection through the fracture. Thus, even in densely fractured media, the cumulative error accrued is likely to be less than 1 per cent, and will in no way influence the shape of the breakthrough curves.

In Figure 6, calculation of the log-log slopes show a linear relationship with a slope of approximately $t^{-3/2}$ below a mass rate of exit of $2{\cdot}5 \times 10^{-4}$ g/day. This is approximately 0·7–9 per cent of the peak rate for porosities of 0·1–1 per cent, respectively. Thus, as matrix porosity increases, the linear slope takes up more of the curve. However, irrespective of matrix porosity, the mass in this range of the curve is a small fraction of the input, which will lead to considerable uncertainty in the concentration in real field situations of this scale. In addition, standing water in the measurement boreholes will dilute the incoming concentrations (e.g. Reference 25) possibly to below detection limit. Therefore, use of the $t^{-3/2}$ slope as an indicator of matrix diffusion may be impractical for most field conditions at this scale.

Figure 6 also illustrates the profound significance of matrix diffusion in a fracture network. Even with porosities typical of crystalline rock environments, the effect of matrix diffusion acts to significantly retard and diminish in concentration, the advancing solute front. For the case illustrated in Figure 6, a porosity of 1 per cent results in retardation of the peak arrival time by 1/2 an order of magnitude and diminishment of peak mass by greater than an order of magnitude. For domains of greater length or of higher fracture density, the effect is even more significant.

Thus, to investigate transport processes in crystalline rock, domain size in relation to fracture density must be considered.

SUMMARY AND CONCLUSIONS

A semi-analytical model is developed in this paper that simulates flow and transport in a network of fractures. The model is developed using the Laplace transform method to eliminate the need for time stepping. Solute transfers at fracture intersections are accomplished using stream tube routing or complete mixing, depending on the hydrodynamics of the fracture intersection. The concentration distribution in the network is determined using a step-wise solution method. The model was shown to be robust and accurate over a wide range of Peclet numbers. To illustrate the use of the model, simulations were conducted using a variety of fracture arrangements both with and without matrix porosity.

The effect of sheeting fractures was simulated using a rudimentary fracture arrangement overlain on a network of smaller aperture fractures. Significant asymmetry in the breakthrough curves was observed. Bi-modal curves were observed for some realizations. The shape of the breakthrough curves was also found to be sensitive to the arrangement of the smaller aperture fractures that interconnect the sheeting fractures. It is surmized that the denser arrangement of sheeting fractures will smooth the breakthrough curves while a sparser arrangement of the interconnecting fractures will increase the irregularity in the shape of the curve.

Several simulations were also conducted using a network of fractures generated using unconditional methods. The results show that, in response to a slug input of solute, the tail of a breakthrough curve at late times may be characterized by a slope of $t^{-3/2}$ in log–log concentration. However, the concentrations in the tail may be too small to observe the slope, depending on the size of the domain. It was also shown that the effect of matrix diffusion is profound, even for very small values of matrix porosity. The migration of solutes in highly fractured rock of low porosity may be so strongly retarded that transport will be limited to the larger sheeting fractures where groundwater velocities are high and mass loss low.

APPENDIX

Notation

$2b$	aperture of the fracture element, L
c	concentration in fracture element,† M/L^3.
c'	concentration in matrix,† M/L^3
D	hydrodynamic dispersion, L^2/T
D'	effective diffusion coefficient within matrix, L^2/T
E	exponential factor for transport processes
F	mass rate of flow,† M/T
J	mass flux,† M/L^2T
L	length of fracture element, L
M	mass of solute,† M
p	Laplace transform of time, 1/T

†May be overlined to indicate that the variable was transformed into the Laplace domain.

Q	volumetric flow, L^3/T
R	retardation factor in fracture element
R'	retardation factor in matrix
t	time, T
V	average linear velocity of groundwater, L/T
w	unit width of fracture, L
x	local co-ordinate parallel to the axis of a fracture element, L
z	local co-ordinate perpendicular to the axis of a fracture element, L
θ	porosity of rock matrix
λ	linear decay constant of solute, 1/T
v	$V/2D$, 1/L
Φ	dimensionless factor for advective flux

Subscripts

(EX)	solute is exiting from the fracture element
(ENT)	solute is entering into the fracture element
i	property of a node
j, $j1$, $j2$, $j3$, $j4$	property of fracture element
in	solute entering a collection of nodes at a given time
out	solute exiting a collection of nodes at a given time
stored	solute stored in the network at a given time
n	upper limit of a summation

ACKNOWLEDGEMENTS

Discussions with Dale Bray, Andrew Piggott, and Ed Sudicky were helpful in developing this model. Funding for this research was provided by Environment Canada.

REFERENCES

1. J. Bear, 'Modeling flow and contaminant transport in fractured rocks', in *Flow and Contaminant Transport in Fractured Rocks*, Academic Press, San Diego, 1993.
2. D. H. Tang, E. O. Frind and E. A. Sudicky, 'Contaminant transport in fractured porous media: analytical solution for a single fracture', *Water Resour. Res.*, **17,** 555–564 (1981).
3. L. Smith and F. W. Schwartz, 'An analysis of the influence of fracture geometry on mass transport in fractured media', *Water Resour. Res.*, **20,** 1241–1252 (1984).
4. M. C. Cacas, E. Ledoux, G. de Marsily, B. Tillie, A. Barbareau, P. Calmels, B. Gaillard, and R. Margritta, 'Modelling fracture flow with a stochastic discrete fracture network: calibration and validation 2.The transport model', *Water Resour. Res.*, **26,** 479–489 (1990).
5. B. Dverstorp, J. Andersson and W. Nordqvist, 'Discrete fracture network interpretation of field tracer migration in sparsely fractured rock', *Water Resour. Res.*, **28,** 2327–2343 (1992).
6. E. A. Sudicky and R. G. McLaren, 'The Laplace transform Galerkin technique for large-scale simulation of mass transport in discretely fractured porous formations', *Water Resour. Res.*, **28,** 499–514 (1992).
7. R. K. Rowe and J. Booker, 'A semi-analytical model for contaminant migration in a regular two- or three-dimensional fractured network: conservative contaminants, *Int. J. Num. Anal. Meth. Geomech.*, **13,** 531–550 (1989).
8. R. K. Rowe and J. Booker, 'A semi-analytical model for contaminant migration in a regular two- or three-dimensional fractured network: reactive contaminants, *Int. J. Numer. Anal. Meth. Geomech.*, **14,** 401–425 (1990).
9. D. Mitchell and E. A. Sudicky, 'Analytical solution for solute transport in a two-dimensional fracture network', *Unpublished Report*, University of Waterloo, 1991 32 pp.

10. J. A. Küpper, F. W. Schwartz and P. M. Steffler, 'A comparison of fracture mixing models. 1. A transfer approach to mass transport modelling', *J. Cont. Hydrol*., **18,** 1–32 (1995).
11. B. Berkowitz, C. Naumann and L. Smith, 'Mass transfer at fracture intersections: an evaluation of mixing models', *Water Resour.. Res.* **30,** 1765–1773 (1994).
12. A. W. Nordqvist Y. Tsang, C.-F. Tsang, B. Dverstorp and J. Andersson, 'A variable aperture fracture network model for flow and transport in fractured rocks', *Water Resour. Res*., **28,** 1703–1713 (1992).
13. A. Rouleau, 'Statistical characterization and numerical simulation of a fracture system: application to groundwater flow in the Stripa granite', *Ph.D. Thesis*, University of Waterloo, 418 pp. 1984.
14. J. A. Barker, 'Reciprocity principle and an analytical solution for Darcian flow in a network', *Water Resour. Res*., **27,** 743–746 (1991).
15. K. S. Novakowski, 'An evaluation of boundary conditions for one-dimensional solute transport, 2, column experiments', *Water Resour. Res*., **28,** 2411–2423 (1992).
16. F. R. De Hoog, J. H. Knight and A.N. Stokes, 'An improved method for numerical inversion of Laplace transforms', *SIAM J. Sci. Statist. Comput*., **3,** 357–366 (1982).
17. A. F. Moench, 'Convergent radial dispersion: a note on evaluation of the Laplace transform solution', *Water Resour. Res*., **27,** 3261–3264 (1991).
18. J. D. Bogan, 'A semi-analytical model for the simulation of solute transport in network of fractures', *M.Sc.E Thesis*, University of New Brunswick, 1996.
19. F. S Barone, R. K. Rowe and R. Quigley, 'Laboratory determination of chloride diffusion coefficient in an intact shale', *Can. Geotech. J*., **27,** 177–184 (1990).
20. F. W. Schwartz, L. Smith and A. S. Crowe, 'A stochastic analysis of macroscopic dispersion in fractured media', *Water Resour. Res*., **19,** 1253–1265 (1983).
21. G. R. Holzhauser, 'Origins of sheet structure, 1. Morphology and boundary conditions', *Engng Geology*, **27,** 225–279 (1989).
22. K. G. Raven, 'Hydraulic characterization of a small ground-water flow system in fractured monzonitic gneiss', *National Hydrology Research Institute Paper* 30, Ottawa, Ontario, 1986, 133pp.
23. C.-E. Klockars, O. Persson and O. Landstrom, 'The hydraulic properties of fracture zones and tracer tests with non-reactive elements in Studsvik', *SKBF/KBS Technical Report* 82–10, Stockholm, Sweden, 1982, 35pp.
24. Y. W. Tsang, 'Study of alternative tracer tests in characterizing transport in fractured rocks', *Geophys. Res. Lett*., **22,** 1421–1424 (1995).
25. K. S. Novakowski, 'The analysis of tracer experiments conducted in divergent radial flow fields', *Water Resour. Res*., **28,** 3215–3225 (1992).

